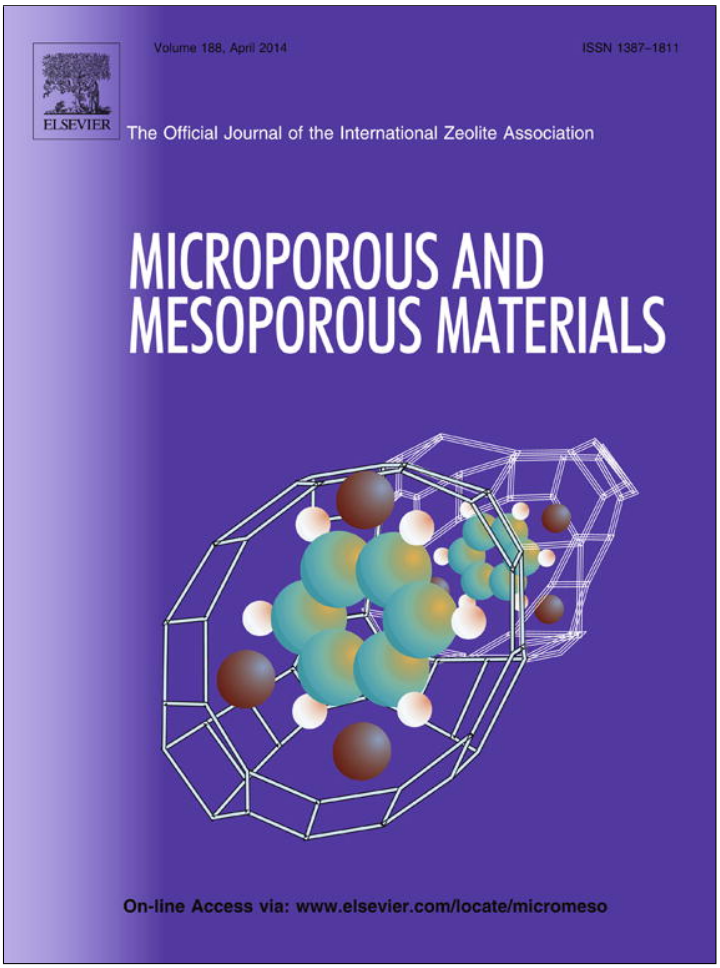

Microporous and Mesoporous Materials 188 (2014) 118–125

Contents lists available at ScienceDirect

Microporous and Mesoporous Materials

journal homepage: www.elsevier.com/locate/micromeso

Antifungal activity of silver ions exchanged in mordenite

Chiericatti Carolina [a], Basílico Juan Carlos [a], Basílico María L. Zapata [a], Zamaro Juan Manuel [b,*]

[a] Cátedra de Microbiología, Facultad de Ingeniería Química, Universidad Nacional del Litoral, Santiago del Estero 2829, 3000 Santa Fe, Argentina
[b] Instituto de Investigaciones en Catálisis y Petroquímica, INCAPE (FIQ, UNL-CONICET), Santiago del Estero 2829, 3000 Santa Fe, Argentina

ARTICLE INFO

Article history:
Received 28 September 2013
Received in revised form 3 December 2013
Accepted 28 December 2013
Available online 8 January 2014

Keywords:
Silver–zeolite
Fungi
XPS
Mordenite
Yeast

ABSTRACT

We investigated the action of silver-exchanged mordenite (Ag–mordenite) against the growth of six fungi that are problematic in the food industry. The mould species studied were *Rhizopus oryzae*, *Mucor circinelloides*, *Geotrichum candidum*, and the yeasts were *Saccharomyces cerevisiae*, *Debaryomyces hansenii* and *Zygosaccharomyces rouxii*. Several instrumental methods (EPMA, XRD, XPS, TPR, AAS) were used for the characterization of Ag–mordenite in order to explain its antifungal activity. Results show that Ag–mordenite exerted an effective antifungal action due to a release of silver ions from the zeolite matrix, which acted directly on the walls of the microorganisms, being more effective than the free silver ions in solution. The yeasts were more sensitive than filamentous fungi, *S. cerevisiae* being the most susceptible specie whereas *G. candidum* was the more resistant.

1. Introduction

The antimicrobial capacity of silver particles is widely known but its effectiveness depends on many factors such as particle size and morphology. In general, since smaller particles have a more effective antimicrobial capacity, several methods have been developed to obtain silver nanoparticles, such as microemulsion, sonochemical reduction and photochemical synthesis [1–3]. On the other hand, nanoparticles tend to aggregate, which leads to a deterioration of their antimicrobial properties, also presenting the problem of their recovery and reuse. This has prompted the study of nanoparticle immobilization in various inorganic materials such as titania [4], silica [5], ceramics [6] or titanium phosphate [7], although this involves the intervention of new factors, namely the mechanical and chemical durability of the supports and their ability to release the nanoparticles. These active nanoparticles may also be silver ions hosted on inorganic matrices which act as vehicles to deliver the ions progressively, such as clays [8], titanosilicates [9] and zeolites [10]. These latter materials have a high exchange capacity, specific surface area, chemical inertness and are not toxic. In particular, mordenite is a zeolite of medium pore size with a 1-dimensional and linear system of channels, consisting of 12-membered rings with an elliptical pore aperture of 7×6.5 Å interconnected to another more closed channel system of 8 members (3.4×4.8 Å) running in the same direction [11]. We have selected this zeolite as a carrier because it has an appropriate Si/Al to allow a good ion exchange capacity and, moreover, because it has been reported that this framework can stabilize different types of cationic silver clusters [12]. In recent years, several types of zeolites containing Ag, Cu or Zn ions and/or nanoparticles applied mainly for antibacterial purposes have been studied [13–29]. In contrast, the literature on the action of Ag–zeolites against fungi is much more limited. We could mention the pioneering work of Ishitani [13] and Nikawa et al. [15], which employed a commercial product named Zeomic® [30], an zeolite A with 2.5% w/w Ag, for the growth control of *Saccharomyces cerevisiae* and *Candida albicans*, respectively. Ferreira et al. [14] and Malachová et al. [16] also showed the good efectiveness of Ag–zeolite Y and Ag–montmorillonite against *S. cerevisiae, C. albicans, Pycnoporus cinnabarinus* and *Pleurotus ostreatus* [16].

Fungi are problematic microorganisms that cause contamination especially in the food industry, provoking significant economic losses. In this context, the purpose of this work is to investigate the antifungal activity of silver-exchanged mordenite, against three yeasts and three molds which were isolated from contaminated food of industrial sources, in low oxygen tension conditions. The properties of the materials were characterized in order to correlate their physicochemical characteristics with their antifungal behavior.

2. Experimental

2.1. Preparation of Ag–mordenite

Na–mordenite (Zeolyst CBV 10A, Si/Al = 6.5) was employed as support, which was ion-exchanged with silver solutions of

* Corresponding author. Tel./fax: +54 0342 4536861.
E-mail address: zamaro@fiq.unl.edu.ar (J.M. Zamaro).

1387-1811/$ - see front matter © 2014 Elsevier Inc. All rights reserved.
http://dx.doi.org/10.1016/j.micromeso.2013.12.033

different concentrations. $AgNO_3$ (Sigma–Aldrich, 99.0% in distilled water) was employed to prepare exchange solutions with concentrations of 0.005, 0.01, 0.025 and 0.1 M. The general conditions were taken considering various ion-exchange procedures for zeolites [31], so as to obtain between 4% and 15% w/w Ag in mordenite. Briefly, 4 g of Na–mordenite (Na–mor) were suspended in the $AgNO_3$ solutions under stirring at room temperature for 24 h in darkness, to avoid reduction of ions to Ag^0. Then, the solids were filtered in darkness and washing twice with 250 ml of distilled water to remove the excess of silver solution. Afterwards, the solids were dried in an oven at 130 °C for 24 h and then stored in ermetic jars in a dry and dark place. Furthermore, $Ag(NO_3)$ solutions were also prepared in such a way as to obtain concentrations of 1670, 555, 170 and 55.4 μM in the culture medium. With these solutions, antifungal assays were performed in order to compare the action of free silver ions in solution with that provided for Ag–mordenite.

2.2. Microorganism isolation and microbiological assays

2.2.1. Isolation of fungi and preparation of inoculum suspension

The moulds employed were isolated from dairy products which presented alterations in conditions of low oxygen tension. The samples were obtained by the method of serial dilutions and seeded in malt extract agar (MEA) (malt extract 2.0%; agar; peptone bacteriological 0.1%, Glucose 2%, w/v in distilled water) with the addition of chloramphenicol (100 mg l^{-1}). The incubations were performed at 25 °C for 5 days and then the fungal flora was identified according to their macroscopic and microscopic characteristics [32,33]. The isolated moulds were *Rhizopus oryzae* Went and Prins. Geerl, *Mucor circinelloides* Tiegh and *Geotrichum candidum* Link: Fr., which were preserved in tubes containing glycerol-water (18% w/w) and stored at −20 °C until completion of the antimicrobial tests. The yeasts were isolated from altered fruit juices contained in plastic bottles, in a similar way as just described. The selected yeasts were *Saccharomyces cerevisiae* Meyen (S.c.) (LMFIQ-701); *Zygosaccharomyces rouxii* (Boutroux) Yarrow (Z.r.) (LMFIQ-702) y *Debaryomyces hansenii* (Zopf) Lodder & Kreger (D.h.) (LMFIQ-700).

In order to prepare the inoculum suspensions, mould spores and yeasts were collected in the late exponential growth phase, poured in sterile tubes containing 5 ml of malt extract broth (MEB) and adjusting the concentrations to 10^4–10^5 spores ml^{-1}.

2.2.2. Fungicidal tests

Assays were performed by suspending 300, 100, 60, 30 or 10 mg of Ag–mordenite containing 5.6% w/w Ag in 100 ml MEB. The suspensions were sonicated for 10 min to homogenize the culture medium and remove the air entrapped in the porosity of the zeolite particles. Then, 9 ml of suspensions were distributed into tubes of 10 ml of capacity with screwcaps, seeded with 1 ml of the fungal inoculum and incubated at 28 °C. Tests were conducted in triplicate under low oxygen tension conditions. Error bars were displayed later in the respective curves. For all the strains, control tests were also conducted without Ag–mordenite or with the addition of Na–mordenite. After the incubation of the microorganisms at different times (0, 1, 2, 4, 6, 8, 12, 24 and 48 h), counts (CFU ml^{-1}) using decimal dilutions were conducted. For this, 1 ml of each suspension was seeded in depth in MEA, the plates were incubated and the counts were obtained in duplicate. For tests with silver solutions we proceeded in the same way as described above, working with concentrations of 1670, 555, 170 and 55.4 mM contained in 9 ml of MEB. The incubations were carried out in darkness.

2.3. Physicochemical characterizations

The X-ray diffraction (XRD) of the solids was performed with a Shimadzu XD-D1 equipment at 2° min^{-1} between $2\theta = 5°$ and 50° using Cu Kα radiation ($\lambda = 1.5418$ Å, 30 kV, 40 mA). The relative crystallinity was estimated considering the integrated area below the main peaks and taking 100% crystallinity for Na–mordenite before ion exchange.

MEB media containing Ag–mordenite were incubated and then filtered with 0.45 μm Sartorius membrane filter to recover the liquid phase. The amounts of silver released into the culture medium were determined by atomic absorption spectroscopy (AAS) with a Perkin Elmer 800 AAnalyst with flame atomization. The amount silver present in Ag–mordenite was also determined by AAS, the solid being previously digested by treating 100 mg of the sample with 10 ml $HClO_4$ + 2 ml HNO_3 on a heating plate for 8 h. Then 2 ml of HF were added and digested for 1 h, diluted and filtered. Temperature-programmed reductions with H_2 (H_2-TPR) were performed with an Ohkura TP-2002S to evaluate the amount and type of silver species. Previously, in situ pretreatments to dry the sample were performed, flowing N_2 at 300 °C and maintaining at this temperature for 30 min. Then, the sample was allowed to cool and changed to a stream of H_2 diluted in He, after which a temperature ramp to 900 °C at 5 °C min^{-1} was applied. H_2 consumption vs sample temperature was recorded and the profiles were deconvoluted to separate individual peaks.

Elemental probe microanalysis (EPMA) was performed to determine the Na/Al and Ag/Al molar ratios in the zeolite with an energy dispersive equipment EDAX coupled to a SEM JEOL JSM-35C. The sample was coated with graphite and X-ray spectra were obtained with an accelerating voltage of 20 kV. Semiquantitative analyses were obtained using the SEMIQ method, which does not require the use of standards.

The oxidation state of the silver surface species was examined with a module Multitechnique Specs equipped with a dual X-ray source Mg/Al and hemispherical analyzer 150 Phoibos in fixed analyzer transmission mode (FAT). We analyzed the binding energies (BE) of Ag 3d, Si 2p, Al 2p, C 1s and O 1s core-levels. The kinetic energy (KE) in the region of the Ag M_4VV Auger transitions was also analyzed and thereby determined the modified Auger parameter ($\acute{\alpha}$), defined as $\acute{\alpha}$ = KE (Ag M_4VV) − KE (Ag $3d_{5/2}$) + 1253.6 eV. The spectra were obtained with a pass energy of 30 eV with a Mg anode operated at 200 W. The pressure during the measurement was less than 2.10^{-8} mbar. The samples were ground, pressed, supported on the sample holder, subjected to vacuum dehydration at 300 °C for 20 min and finally evacuated under vacuum prior to the readings. The Si 2p peak of the zeolite at 102.4 eV binding energy (BE) was taken as internal reference. Data processing and peak deconvolution were performed using the Casa XPS software.

3. Results and discussion

3.1. Physicochemical characterizations

3.1.1. Compositional studies by AAS and EPMA

Table 1 shows the different Ag–mordenite samples obtained after the ion- exchange processes. By AAS it was determined that solids containing 3.9%, 5.6%, 10.3% and 13.6% w/w of silver were obtained, which were designated as Ag(4)Z, Ag(6)Z, Ag(10)Z, Ag(14)Z, respectively. It is observed that the silver loading in the zeolite increased and, at the same time, the sodium content decreased as the concentration of the exchange solution was higher (indicated between brackets). Table 1 also shows that the Ag/Al and Na/Al atomic ratios, as determined by EPMA, exhibited the

Table 1
Silver loading, elemental composition, relative crystallinity and exchange degree of Ag–mordenite samples and Na–mordenite support.

Sample	Ag (% w/w) [a]	Na (% w/w) [a]	Na/Al [b]	Ag/Al [b]	Crystallinity (%) [c]	Exchange % [d]
Ag(14)Z [0.1]	13.6	0.2	–	1.05	63	88.0
Ag(10)Z [0.025]	10.3	1.2	0.01	0.84	80	64.2
Ag(6)Z [0.01]	5.6	2.3	0.04	0.47	98	33.1
Ag(4)Z [0.005]	3.9	3.3	0.12	0.31	100	25.6
Na–mor	–	4.6	0.26	–	100	0

[a] Determined by AAS.
[b] Determined by EPMA.
[c] Determined by XRD.
[d] Estimated as follows: the unit cell of mordenite is $Na_xAl_xSi_yO_{96}{\cdot}24\ H_2O$, where $x + y = 48$. The Si/Al measured in the Ag(14)Z sample was Si/Al = 5.73. If Si/Al = 5.7 then $y = 42.4$. The composition was $Na_{5.7}Al_{5.7}Si_{42.4}O_{96}{\cdot}24\ H_2O$ (formular weight = 3437.92 g mol^{-1}). The percentage was estimated with the mmol of Ag in each sample, considering that 5.7 mmol correspond to a 100% of exchange.

same trends as the silver and sodium content taking into account that the amount of aluminum in the zeolite remained constant. Both results confirm the effectiveness of the silver ion exchange process. It should be noted that a small amount of Na was detected by AAS in the sample with higher silver content, which was not observed by EPMA because it was under the detection limit of this technique. Considering the silver loading, the Si/Al ratio and the formular weight of this zeolite (see footnote), an exchange level was estimated for each sample. It can be seen that in the sample with higher loading a high, but not total, exchange level was reached.

On the other hand, tests to determine the amount of silver released into the culture medium were conducted in some of these samples. Incubation conditions similar to those later used in the microbiological tests were adopted. Ag–mordenite samples were put in contact with MEB, and the silver released to liquid media at different periods was determined by AAS (Table 2). It can be seen that for Ag(6)Z (test performed in duplicate on two different samples), the amount of released silver was low and remained constant throughout the period under study. The assay with the Ag(4)Z sample showed a similar trend, but the amount of silver released to the solution was about 3 times lower as above. These results show that despite the considerable amount of silver loaded in these samples, its release in the culture medium was very low in the absence of microorganisms.

3.1.2. Structural studies by XRD and H_2-TPR

Through XRD, the crystalline structure of mordenite samples after the ion-exchange process was evaluated. The diffractogram of the Na–mor support (Fig. 1) shows a pure material with high crystallinity, all diffraction peaks corresponding to those indexed for this zeolite [11]. When the zeolite was ion exchanged under the more drastic conditions, i.e. using the solution of higher silver concentration, the main crystalline structure of the zeolite was maintained (Fig. 1). However, a gradual decrease was observed in the relative intensity (relative to the other diffraction peaks) of the peak at $2\theta = 9.6°$, corresponding to (200) planes, as the silver content in the solid increased. It has been reported for Ag–clinoptilolite that variations in the relative intensities of the (020) and (200) planes after the ion-exchange are due to the nature, location and amount of extra-framework species [34]. In that case, the lower intensity of the (020) signal was associated with extra-framework silver species located in the mirror plane, perpendicular to the *b*-axis [35]. Since in mordenite the main channels run along the b-direction, the predominant incorporation of silver species according to this orientation would be the consequence of the decrease in the XRD intensity of the said planes, while others remain unchanged. No metallic silver was detected. Moreover, there was a partial loss of crystallinity of mordenite which was greater when the silver content increased (Table 1). This loss could be due to intracrystalline distortions caused when large amounts of metal are introduced in the mordenite channels [36].

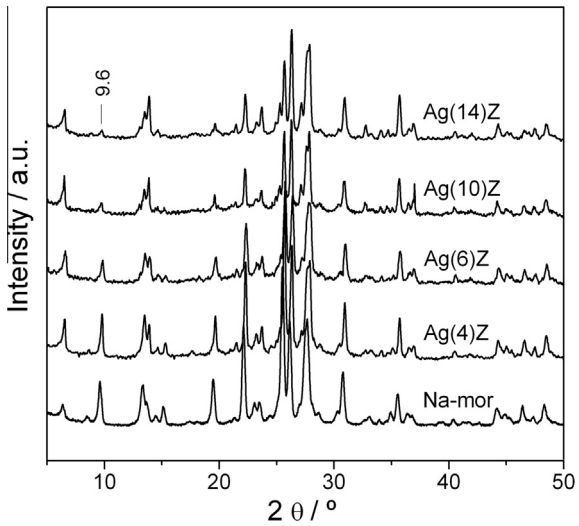

Fig. 1. X-ray diffraction patterns of Ag–mordenites with different silver loadings.

Table 2
Amounts of silver released to the culture medium at different times.

Sample	Time (h)				
	0	3	5	9	48
	Ag in solution (ppm)				
$Ag(6)Z_a$	15	16	13	18	–
$Ag(6)Z_b$	18	–	–	17	17
Ag(4)Z	3	4	8	4	–

In order to analyze the nature of the silver species present in the samples, H_2-TPR characterizations were performed. Fig. 2 shows that as the silver loading increases, the overall profile is maintained but with a gradual increase in the intensity of the peaks, according to a higher amount of reducible species. All the profiles were qualitatively similar and four regions were well defined, except for the sample with the highest loading. It has been reported that in mordenite the exchangeable ions are located at three types of sites [37]: α sites at the main channel and coordinated with oxygen atoms of the zeolite network, β sites at the 8-membered ring adjacent to the main channel; and γ sites located in small cavities of the mordenite. In the latter, the metal has an octahedral coordination, being the site with the higher coordination. According to the observed profiles, the peaks centered at ~115 °C are assigned to the partial reduction of low-interaction Ag^+ ions, located inside the main channel (α sites), to $Ag_n^{\delta+}$ clusters, which are then reduced at higher temperatures [38]. For the Ag(14)Z sample, a new maximum was observed at 160 °C due to the reduction of highly

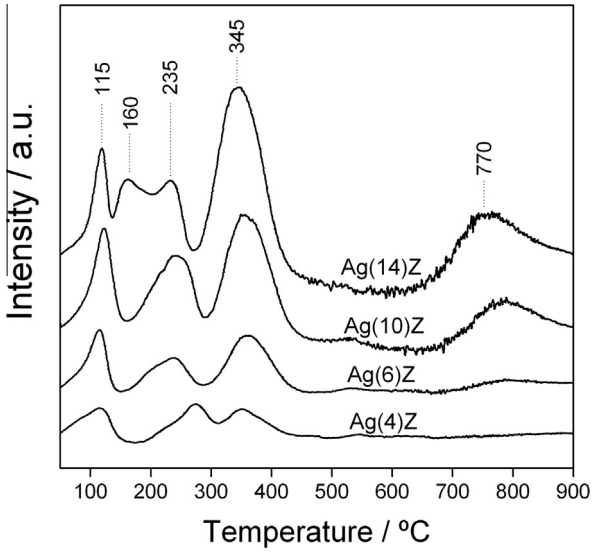

Fig. 2. H_2-TPR profiles of Ag–mordenites.

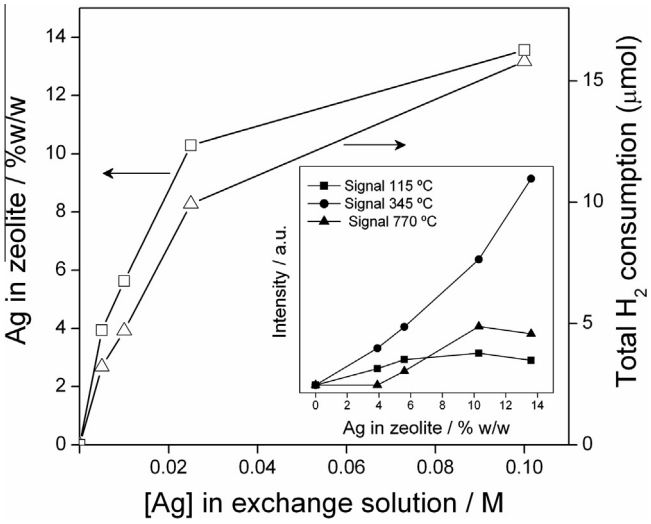

Fig. 3. Total H_2 consumption against the concentration of the $AgNO_3$ exchange solution. The inset shows the consumption of different species against the metal loading in the zeolite.

dispersed Ag_2O species on the surface of the zeolite crystals, coming from extra-framework species present in this sample with high metal loading. This is in agreement with H_2-TPR studies of mechanical mixtures of this oxide and Na–mordenite [39]. The peak at 235 °C is assigned to the complete reduction of $Ag_n^{\delta+}$ clusters in α sites, whereas the peak at 345 °C is originated by the reduction of Ag^+ species in β sites, somewhat more stables. Finally, the peak above 700 °C is due to the reduction of Ag^+ species in the more stables γ sites. At these locations the ions interact strongly with the structure of the zeolite being less reducible. These species start to insinuate in the Ag(6)Z sample. As an overview of the TPR profiles, it can be said that there are several cationic silver species with different interactions with the mordenite matrix.

The total H_2 consumption (Table 3) matches well with the results of the metal content, considering that normally not all the metal dispersed in a zeolite is subjected to be reduced. Furthermore, the incorporation of silver in mordenite follows the same trend as the H_2 consumption (Fig. 3). The inset of Fig. 3 shows the trends in the main peaks as a function of the silver content in the zeolite and it can be seen that the amount of species at α and β sites grew from the beginning, then the α saturated while γ started to appear. The maximum molar ratio between Ag^+ and H_2 is 0.5. Note that this ratio increased from about 0.3–0.42 for the sample with higher silver content (Table 3), probably because of the presence of some amount of oxide, which is more easily reducible in this latter sample.

3.1.3. Surface species studied by XPS

Table 4 shows the binding energies (BE) of the electronic transitions of Ag $3d_{5/2}$ core levels in Ag–mordenite samples which are centered around 368 eV. A review of the BE data of these transitions for different types of silver oxides and metallic silver compiled in the NIST database [40] as well as in many published papers shows a dispersion and even an overlap of those values, ranging from 367.9 to 368.4 for Ag^0, 367.6 to 368.5 for Ag_2O and 367.3 to 368.1 for AgO [41]. This means that the oxidation states of the silver species are difficult to determine by analyzing only the BE shifts. However, for the sample with higher silver content a clear BE shift can be seen, which allows identifying two components, one centered at 367.8 eV which is compatible with the presence of silver oxides (Fig. 4a). A better differentiation of the oxidation states can be achieved by calculating the modified Auger parameter (ά), which considers the kinetic energy (KE) of the M_4VV Auger transitions and is defined as ά (eV) = KE (Ag M_4VV) − KE (Ag $3d_{5/2}$) + 1253.6 eV. This parameter allows one to clearly differentiate Ag^0 (726.3) of their oxides, AgO and Ag_2O (724.7 and 724.5 eV, respectively [42]. Meanwhile, for Ag ions exchanged in zeolites, ά is found around 724 eV similarly to Ag^+ salts, making it possible to differentiate these cationic species from other silver oxides or metallic silver [14,39].

The profile of the spectra in the AgMVV Auger region shows a complex structure (Fig. 4b) assigned to AgM_4VV and AgM_5VV electron transitions [42,43]. In the Ag–mordenite samples with low metal content, such peaks can be deconvoluted into two main components, while in the sample with a higher loading four components are necessary. In the former, the KE of AgM_4VV are around 355 eV (Table 4), while for Ag(14)Z, in addition to this peak, there appeared another around 357 eV. The ά values clearly show that in all samples there are only Ag^+ ions in the surface of zeolite network, except for the Ag(14)Z sample in which there is also a certain amount of Ag_2O, generated from extra-framework species after the thermal pretreatment for XPS measurements.

Table 3
H_2-TPR results for Ag–mordenite samples.

Sample	Total H_2 consumption (μmol)	Ag content (mg)	Ag loading (% w/w)	H_2/Ag
Ag(4)Z	3.22	0.54	2.3	0.29
Ag(6)Z	4.70	0.79	3.4	0.30
Ag(10)Z	9.93	1.66	6.9	0.34
Ag(14)Z	15.81	2.64	11.3	0.42

Table 4
XPS results: binding energies (BE), kinetic energies (KE), modified Auger parameters (ά) and surface elemental composition of Ag–mordenites.

Sample	BE Ag $3d_{5/2}$ (FWHM)[a]	KE Ag $3d_{5/2}$[a]	KE Ag M_4VV[a]	ά[b]	Si/Al	Ag/Al	Na/Al
Ag(4)Z	368.1(2.0)	885.4	355.9	724.0	5.9	0.19	0.75
Ag(6)Z	368.3(1.9)	885.3	355.9	724.1	5.8	0.39	0.43
Ag(10)Z	368.4(1.9)	885.1	355.4	723.8	5.8	0.83	0.12
Ag(14)Z	367.8(1.6)	885.8	357.8	725.5	5.8	2.18	0.06
	368.4(1.9)	885.1	355.7	724.2			

[a] Binding energy (BE) and kinetic energy (KE) in eV.
[b] Modified Auger parameter: ά = KE (Ag M_4VV) − KE (Ag $3d_{5/2}$) + 1253.6 eV.

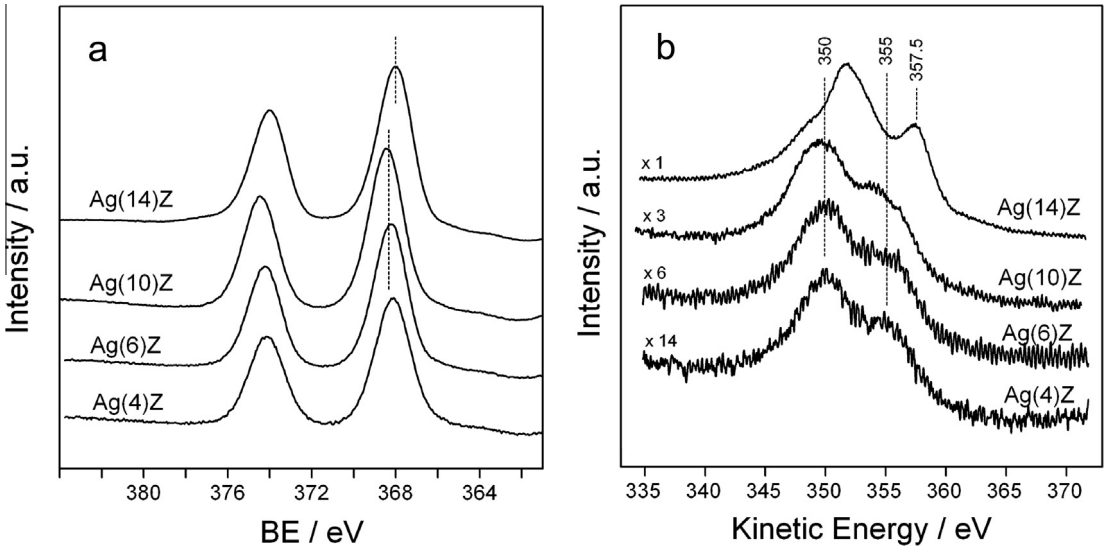

Fig. 4. XPS spectra of Ag–mordenites: (a) intensity of Ag 3d core level transitions as a function of binding energy (BE) and (b) intensity of AgMVV transitions as a function of kinetic energy (KE).

The results of XPS, XRD and TPR indicate that under these preparation conditions of Ag–mordenite, without using severe heat treatments, cationic silver species are obtained in samples containing up to 10% w/w Ag. Metallic silver has been observed in silver–zeolites containing high metal loadings [39,44] when calcinations of the samples were performed during preparation. When a zeolite contains segregated Ag_2O, a high temperature treatment in air atmosphere promotes its decomposition, forming metallic silver. This occurs because the $\Delta G_{(T)}$ for the reaction: $Ag_2O \rightarrow 2Ag + {}^1/_2\, O_2$ becomes negative when the temperature exceeds 500 °C. Consistent with this, in our non-calcined samples, the presence of metallic silver was not observed.

It is also interesting to note that the Na/Al ratio on the most external surface layer of the zeolite crystals decreases monotonically while the Ag/Al ratio increases, as the silver loading increases. However, a surface silver enrichment is observed in the sample with higher loading which is compatible with a surface oxide segregation, whereas a small amount of Na is still observed. These surface characteristics are similar to those found in the bulk of the materials as determined by EPMA and TPR. Moreover, the Si/Al ratio on the surface matches well with that of the bulk of the zeolite (see Table 1), indicating no dealumination process of the zeolite during exhange.

Considering that the Ag(6)Z solid contains an adequate amount of silver incorporated in the zeolite framework exclusively as highly dispersed cationic forms, this material was selected to perform the microbiological assays.

3.2. Antifungal studies

3.2.1. Assays with filamentous fungi

First, we performed experiments using $AgNO_3$ solutions in order to evaluate the action of free silver ions against the various microorganisms tested. When using a concentration of 1670 μM, mold growth was completely inhibited at time zero for all microorganisms. Meanwhile, by employing 555 μM, the growth of *M. circinelloides* and *R. oryzae* was completely inhibited after 2 h (Fig. 5a and b). These reductions in the colonies growth by a factor of 4 Log is considered a significant inhibition degree. For this silver concentration, the CFU ml^{-1} of *G. candidum* decreased 3 Log after 48 h of incubation (Fig. 5c). When lower concentrations of silver were used (170 and 55.4 μM), both *M. circinelloides* and *R. oryzae* showed an effective inhibition, reducing their growth by a factor of 4 Log after 48 h.

Fig. 5d–f shows the curves corresponding to the antifungal tests employing the Ag(6)Z solid. These assays were performed adding different amounts of Ag(6)Z in such a way as to obtain the same amounts of silver into the culture media as those employed in the tests with $AgNO_3$ solutions, as discussed above. Using a ratio of 300 mg Ag(6)Z/100 ml MEB, the growth of the three molds was completely inhibited at $t = 0$. Meanwhile, using 100 mg Ag(6)Z/100 ml MEB, a very good inhibitory action against *M. circinelloides* (Fig. 5d) and *R. oryzae* (Fig. 5e) was observed, reducing 4 Log at 6 and 12 h, respectively. This performance implies a faster antifungal activity of Ag–mordenite compared to free silver ions. *G. candidum* colonies decreased 1.4 Log at 48 h (Fig. 5f) showing, as in the case of Ag^+ in solution, a lower sensitivity against Ag–mordenite. When 60 mg Ag(6)Z/100 ml MEB were employed, both *M. circinelloides* and *R. oryzae* decreased 4 Log of CFU ml^{-1} at 12 and 24 h, respectively, but with a slower rate, whereas for *G. candidum* the CFU ml^{-1} decreased only 0.6 Log after 48 h. It can be speculated that septate molds are more resistant against the action of silver ions than the non-septate molds (Mucorales), but a greater number of species should be tested to confirm this hypothesis. It should be noted that an antimicrobial is considered safe for the food industry when a reduction of 4 Log (99.99% death efficiency) for mold and 5 Log for bacteria [45] is achieved.

3.2.2. Assays with yeasts

For these fungi, tests with $AgNO_3$ solutions were also performed, showing a complete inhibition at time zero for the three genera of yeasts when a silver solution of 1670 μM (not shown) was employed, while for 555 μM the growth of the three microorganisms also showed a complete inhibition but after 2 h (Fig. 6). When solutions of 170 and 55.4 μM were employed, only a lower growth with respect to the control curves for *Z. rouxii* and *D. hansenii* was observed, while for *S. cerevisiae* some degree of inhibition was noticed, accounting for their higher sensitivity to free silver ions. However, compared with molds, $AgNO_3$ solutions were less effective against yeasts.

When assays employing Ag–mordenite were conducted (Fig. 6d–f) using 300 mg Ag(6)Z/100 ml MEB, the yeasts growth was inhibited completely at $t = 0$, while for 100 mg Ag(6)Z/100 ml MEB the colonies reduced 4 Log at $t = 0$, proving that Ag–

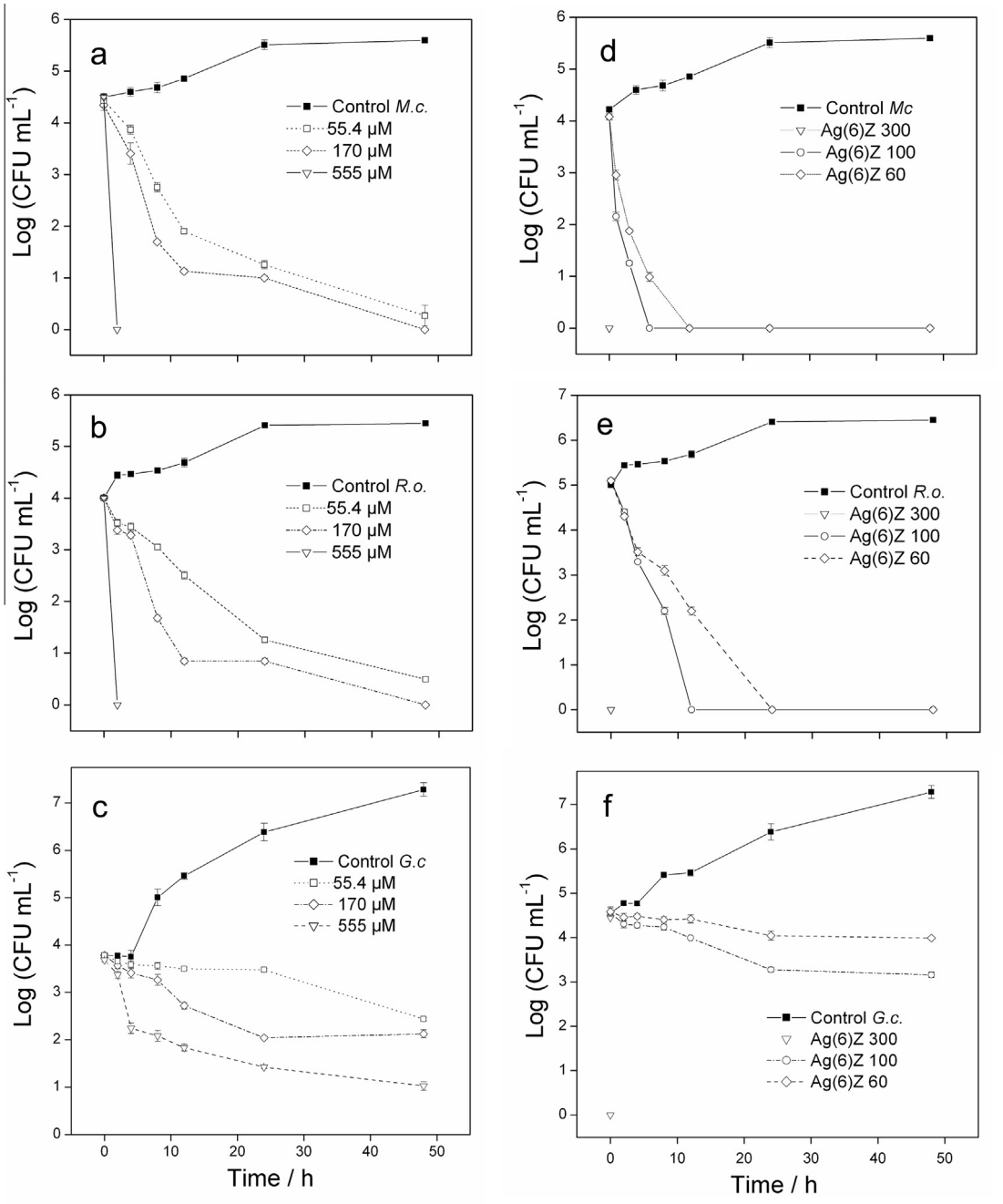

Fig. 5. Growth curves for moulds. Assays employing $AgNO_3$ for: (a) *Mucor circinelloides*; (b) *Rhizopus oryzae*; (c) *Geotrichum candidum*. Assays employing Ag(6)Z for: (d) *Mucor circinelloides*; (e) *Rhizopus oryzae*; (f) *Geotrichum candidum*.

mordenite is effective in small quantities. It should be emphasized that the results obtained with Na–mordenite (100 mg/100 ml MEA) showed a behavior similar to that of the control curves for all microorganisms (mould and yeasts), indicating that the zeolitic support has no inhibitory effect by itself. Furthermore, when a proportion of 60 mg Ag(6)Z/100 ml MEB was used, a strong inhibitory action for the three yeasts was observed, whereas with 30 mg Ag(6)Z/100 ml MEB, the colonies of *Z. rouxii* were reduced in 4 Log after 6 h (Fig. 6d). Afterwards, experiments using only 10 mg Ag(6)Z/100 ml were performed, and a decrease in the CFU ml^{-1} of 4 Log was produced after 24 h. These results show a very effective action of Ag(6)Z when compared with those obtained with silver solutions. In the case of *D. hansenii* (Fig. 6e) a high sensivity was also observed, inhibiting 4 Log after 10 h with 30 mg of Ag(6)Z and reaching the same value of inhibition with 10 mg of Ag(6)Z, but after 24 h. For *S. cerevisiae* (Fig. 6f), the addition of only 10 mg Ag(6)Z/100 ml MEB caused a reduction of 4.5 Log CFU ml^{-1} in 4 h, indicating a strong effect in a short period.

3.2.3. Mode of action of Ag–mordenite against fungi

The physicochemical characterizations showed that Ag(6)Z is composed of cationic silver species incorporated at exchange positions in mordenite and in interaction with it, whereas the zeolite structure was preserved. Therefore, these species can diffuse through the micropores of the zeolite network and interact with the cell walls of the fungi. Moreover, the diversification of the Ag^+ species present may be beneficial for a gradual and controlled dosage of ions, depending on the interaction with the matrix. It has

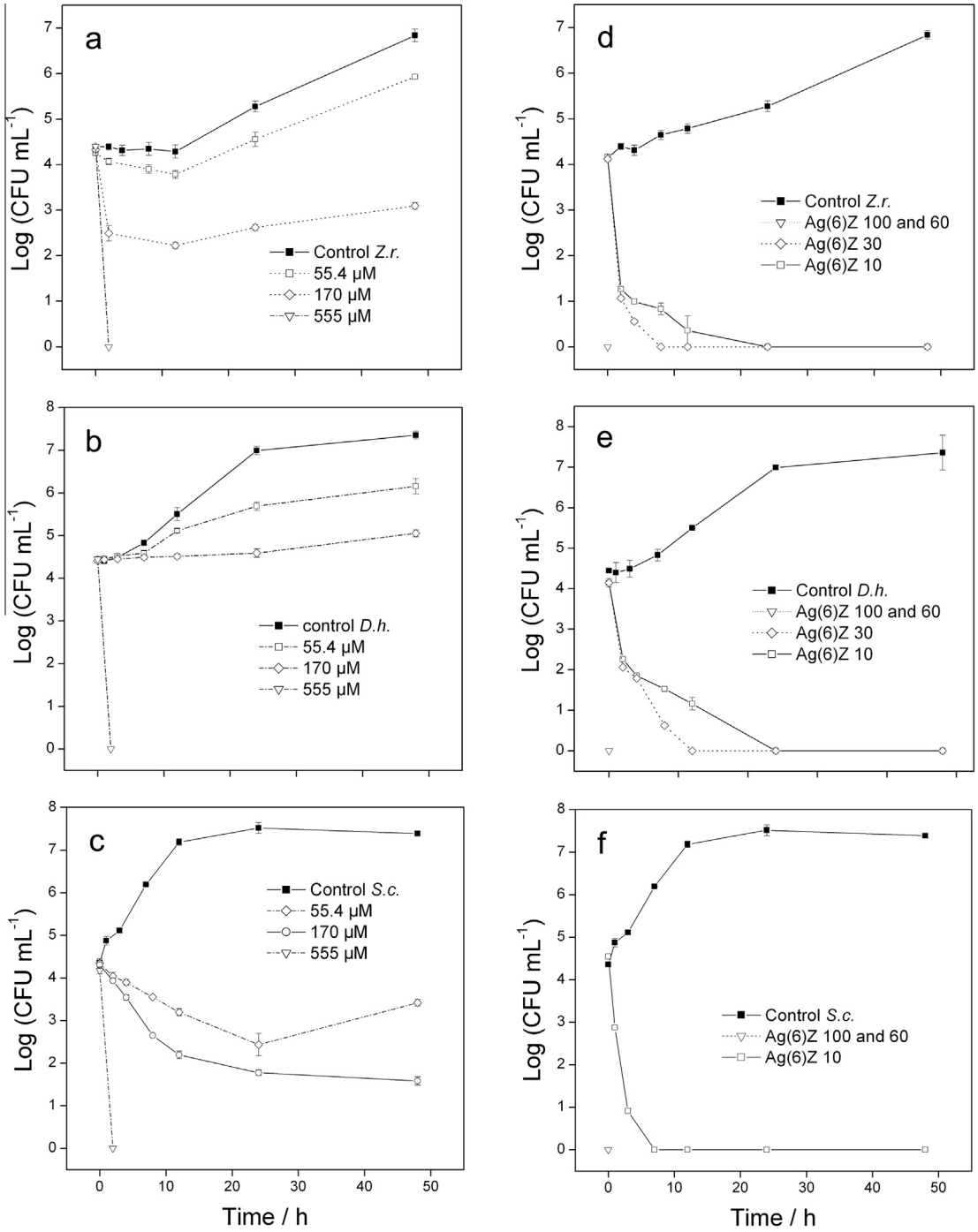

Fig. 6. Growth curves for yeasts. Assays employing $AgNO_3$ for: (a) *Zygosaccharomyces rouxii*; (b) *Debaryomyces hansenii*; (c) *Saccharomyces cerevisiae*. Assays employing Ag(6)Z for: (d) *Zygosaccharomyces rouxii*; (e) *Debaryomyces hansenii*; (f) *Saccharomyces cerevisiae*.

been shown [21] that Ag–zeolites in contact with distilled water release a very low or null amount of silver, the presence of ions in the culture medium being necessary. Moreover, Matsumura et al. [19] determined that the release of silver into a culture medium is much more marked in the presence of a microorganism (bacteria), whereby the action of the silver would be more direct, needing the contact between Ag–zeolite and the microorganism. The latter was also supported by studies of Ishitani [13] and Kwakye-Awuah et al. [17], who found that the amount of silver released by a Ag–zeolite in a medium may vary with microorganism species. This interaction Ag–zeolite/microorganism could be induced by electrical charges on the surface of both materials. In this regard, it has been determined that the Z potential of mordenite has negative values at low pH, whereas the walls of the bacteria also possess weak negative charges but under mildly acidic or neutral conditions bacteria-zeolite adsorption phenomena can occur [46]. It is possible that such phenomena also play a key role in the interaction between the Ag–mordenite crystals and the walls of the fungi studied, which in turn also have differences between them. Since Ag(6)Z contains highly dispersed silver ions and the microbiological assays were performed at low oxygen tension, it is assumed that the antifungal action is due to cationic forms of silver released directly to the cell walls. For bacteria, it has been proposed that silver ions have affinity for the sulfhydryl

groups exposed on the cell walls, resulting in stable S–Ag groups, which inhibits the H_2 transfer [47]. However, the interaction of ions with fungi is different, since the latter require low concentrations of some metal ions for their growth, such as Cu^{+} or Zn^{+2}, which must be transported through the ion entry system. This mechanism could also act for Ag^{+} which has an atomic radius similar to the above and, in addition, it has a higher electronegativity. However, there is little information on the action mechanism of Ag^{+} against fungi, as well as on the different sensitivities exhibited by different fungal species. But generally, it has been suggested that there is a great variability in the response of yeasts and molds to biocides, fungi being usually more resistant to these agents than nonsporulating bacteria (except mycobacteria) [48].

The above discussed results show that the antifungal action of Ag–mordenite was much more effective with respect to free silver ions in solution suggesting the existence of a close interaction between the solid and the wall of the fungi. This contact would facilitate a direct and more efficient dosage of ions. Moreover, when using free silver ions in solution, these ions may be complexed by some ingredients of the culture medium, then reducing the bioavailable Ag^{+} to interact with the fungi. In this sense, it is known that several amino acids and proteins present in a synthethic medium, as L-cysteine, L-methionine, L-histidine, L-tryptophan or albumin can inhibit the action of silver ions in solution [19]. In contrast, when silver ions are encapsulated in the mordenite matrix they are probably protected from these factors, allowing a higher bioavailability to interact with the fungi walls.

4. Conclusion

The antifungal activity of Ag-exchanged mordenite exerted against various isolates of fungal that develop under low oxygen tension was investigated. The preparation conditions made it possible to stabilize cationic silver species exchanged in mordenite, while preserving the framework of the zeolite. A material containing 6% w/w silver presented a very effective action against six fungi which are problematic in the food industry. This action is provided solely by cationic silver species present in the zeolite, which are dosed directly into the walls of the microorganisms. This effect is much more pronounced with respect to equivalent amounts of silver in solution as $AgNO_3$. This is probably because the ions are preserved by the zeolite matrix, avoiding their complexation and because of a close interaction between Ag–mordenite and the microorganism. The effectiveness of inhibition was much more pronounced for yeasts, particularly *S. cereviseae*, while fungi showed a greater resistance, particularly *G. candidum*. This study shows that Ag-exchanged mordenite is an effective biocide agent against a variety of fungi of importance in the food industry.

Acknowledgments

The authors wish to acknowledge the financial support received from Consejo Nacional de Investigaciones Científicas y Técnicas (CONICET), Agencia Nacional de Promoción Científica y Tecnológica (ANPCyT) and Universidad Nacional del Litoral (UNL). Thanks are also given to ANPCyT for the purchase of the UHV Multi Analysis System (PME 8-2003), to Elsa Grimaldi for the English language editing and to Lic. Fernanda Mori for the XPS analyses.

References

[1] Y.D. Yin, Z.Y. Li, Z.Y. Zhong, B. Gates, Y.N. Xia, S. Venkateswaran, J. Mater. Chem. 12 (2002) 522–527.
[2] J. Zhu, S. Liu, O. Palchik, Y. Koltypin, A. Gedanken, Langmuir 16 (2000) 6396–6399.
[3] V.K. Sharma, R.A. Yngard, Y. Lin, Adv. Colloid Interface Sci. 145 (2009) 83–96.
[4] Q. Cheng, C. Li, V. Pavlinek, P. Saha, H. Wang, Appl. Surf. Sci. 252 (2006) 4154–4160.
[5] M. Kawashita, S. Tsuneyama, F. Miyaji, T. Kokubo, H. Kozuka, K. Yamamoto, Biomaterials 21 (2000) 393–398.
[6] V.A. Oyanedel-Craver, J.A. Smith, Environ. Sci. Technol. 42 (2008) 927–933.
[7] Q. Wang, H. Yu, L. Zhong, J. Liu, J. Sun, J. Shen, Chem. Mater. 18 (2006) 1988–1994.
[8] F. Ohashi, A. Oya, L. Duclaux, F. Beguin, Appl. Clay Sci. 12 (1998) 435–445.
[9] L. Lu, Y. Luo, W.J. Ng, X.S. Zhao, Microporous Microporous Mater. 120 (2009) 304–309.
[10] M. Rivera-Garza, M.T. Olguín, I. García-Sosa, D. Alcántara, G. Rodríguez-Fuentes, Microporous Microporous Mater. 39 (2000) 431–444.
[11] Structure Comission of the International Zeolite Association, <http://www.iza.structure.org/database>, 2013.
[12] N. Bogdanchikova, V. Petranovskii, S. Fuentes, E. Paukshits, Y. Sugi, A. Licea-Claverie, Mater. Sci. Eng. A 276 (2000) 236–242.
[13] T. Ishitani, in: P. Ackerman, M. Jagerstad, T. Ohlsson (Eds.), Food and Food Packaging Materials–Chemical, Interactions, Royal Society of Chemistry, Cambridge, 1995, pp. 177–188.
[14] L. Ferreira, A. Fonseca, G. Botelho, C. Almeida-Aguiar, I. Neves, Microporous Mesoporous Mater. 160 (2012) 126–132.
[15] H. Nikawa, T. Yamamoto, T. Hamada, M.B. Rahardjo, H. Murata, S. Nakanoda, J. Oral Rehabil. 24 (1997) 350–357.
[16] K. Malachová, P. Praus, Z. Rybková, O. Kozák, Appl. Clay Sci. 53 (2011) 642–645.
[17] B. Kwakye-Awuah, C. Williams, M. Kenward, I. Radecka, J. Appl. Microbiol. (2007) 1364–5072.
[18] P. Lalueza, M. Monzón, M. Arruebo, J. Santamaría, Mater. Res. Bull. 46 (2011) 2070–2076.
[19] Y. Matsumura, K. Yoshikata, S. Kunisaki, T. Tsuchido, Appl. Environ. Microbiol. 69 (2003) 4278–4281.
[20] J. Hrenovic, J. Milenkovic, I. Goic-Barisic, N. Rajic, Microporous Mesoporous Mater. 169 (2013) 148–152.
[21] Y. Inoue, M. Hoshino, H. Takahashi, T. Noguchi, T. Murata, Y. Kanzaki, M. Sasatsu, J. Inorg. Biochem. 92 (1) (2002) 37–42.
[22] K. Krishnani, Y. Zhang, L. Xiong, Y. Yan, R. Boopathy, A. Mulchandani, Bioresour. Technol. 117 (2012) 86–91.
[23] T. Matsuura, Y. Abe, Y. Sato, K. Okamoto, M. Ueshige, Y. Akagawa, J. Dent. 25 (1997) 373–377.
[24] N. Flores-Lopez, J. Castro-Rosas, R. Ramirez-Bon, A. Mendoza-Cordova, E. Larios-Rodriguez, M. Flores-Acosta, J. Mol. Struct. 1028 (2012) 110–115.
[25] A. Top, S. Ülkü, Appl. Clay Sci. 27 (2004) 13–19.
[26] I. De la Rosa-Gómez, M. Olguín, D. Alcántara, J. Environ. Manage. 88 (2007) 853–863.
[27] S. Magana, P. Quintana, D. Aguilar, J. Toledo, C. Angeles-Chavez, M. Cortes, R. Sánchez, J. Mol. Catal. A – Chem. 281 (2008) 192–199.
[28] K. Kawahara, K. Tsuruda, M. Morishita, M. Uchida, Dent. Mater. 16 (2000) 452–455.
[29] T. Haile, G. Nakhla, Biodegradation 21 (2010) 123–134.
[30] Sinanen Zeomic Co., Ltd., <http://www.zeomic.co.jp/english>, 2013.
[31] G.B.F. Seijger, P. Van Kooten Niekerk, P. Krishna, H.P.A. Calis, H. Van Bekkum, C.M. Van den Bleek, Appl. Catal. B Environ. 40 (2003) 31–42.
[32] R.A. Samson, J. Houbraken, U. Thrane, J.C. Frisvad, B. Andersen, Food and Indoor Fungi, CBS-KNAW Fungal Biodiversity Centre, Utrecht, The Netherlands, 2010.
[33] J.I. Pitt, A.D. Hocking, Fungi and Food Spoilage, third ed., Blackie Academic & Professional, London, 2009.
[34] B. Concepción-Rosabal, G. Rodríguez-Fuentes, N. Bogdanchycova, P. Bosch, M. Avalos, V.H. Lara, Microporous Mesoporous Mater. 86 (2005) 249–255.
[35] O.E. Petrov, in: D.W. Ming, F.A. Mumpton (Eds.), Natural Zeolites '93: Occurrence, Properties and Use, 1995, pp. 271–279.
[36] R.M. Serra, E.E. Miró, M.K. Sapag, A.V. Boix, Microporous Mesoporous Mater. 138 (2011) 102–109.
[37] D. Kaucký, A. Vondrová, J. Dedecek, J. Catal. 194 (2000) 318–329.
[38] J. Shibata, Y. Takada, A. Shichi, S. Satokawa, A. Satsuma, T. Hattori, Appl. Catal. B Environ. 54 (2004) 137–144.
[39] S. Aspromonte, R. Serra, E. Miró, A. Boix, Appl. Catal. A Gen. 407 (2011) 134–144.
[40] NIST X-ray Photoelectron Spectroscopy Database, <http://srdata.nist.gov/xps>, 2013.
[41] A.M. Ferraria, A.P. Carapeto, A.M. Botelho do Rego, Vacuum 86 (2012) 1988–1991.
[42] G.I.N. Waterhouse, G.A. Bowmaker, J.B. Metson, Appl. Surf. Sci. 183 (2001) 191–204.
[43] A. Naydenov, P. Konova, P. Nikolov, F. Klingstedt, N. Kumar, D. Kovacheva, P. Stefanov, R. Stoyanova, D. Mehandjiev, Catal. Today 137 (2008) 471–474.
[44] A.M. Fonseca, I.C. Neves, Microporous Mesoporous Mater. 181 (2013) 83–87.
[45] G. Sapers, Food Technol. Biotech. 39 (4) (2001) 305–311.
[46] M. Kubota, T. Nakabayashi, Y. Matsumoto, T. Shiomi, Y. Yamada, K. Ino, H. Yamanokuchi, M. Matsui, T. Tsunoda, F. Mizukami, K. Sakaguchi, Colloid Surf. B 64 (2008) 88–97.
[47] R.L. Davies, S.F. Etris, Catal. Today 36 (1997) 107–114.
[48] A.D. Russell, W.B. Hugo, G.A.J. Ayliffe, Desinfection, Preservation and Sterilization, Blackwell Scientific Publicationsm, Oxford, UK, 1992.